Title
Effect of nearby piles and soil properties on thermal behaviour of a field-scale energy pile

Journal
Canadian Geotechnical Journal, 58(9)

ISSN
0008-3674

Authors
Moradshahi, Aria
Faizal, Mohammed
Bouazza, Abdelmalek
et al.

Publication Date
2021-09-01

DOI
10.1139/cgj-2020-0353

Peer reviewed

Canadian Science Publishing | Canadian Geotechnical Journal

Effect of nearby piles and soil properties on the thermal behaviour of a field-scale energy pile

Journal:	*Canadian Geotechnical Journal*
Manuscript ID	cgj-2020-0353.R2
Manuscript Type:	Article
Date Submitted by the Author:	19-Oct-2020
Complete List of Authors:	Moradshahi, Aria; Monash University, Civil Engineering Faizal, Mohammed; Monash University, Civil Engineering Bouazza, Abdelmalek; Monash University, McCartney, John; University of California San Diego, Structural Engineering
Keyword:	Energy Piles, Thermal Interaction, Field tests
Is the invited manuscript for consideration in a Special Issue? :	Not applicable (regular submission)

Effect of nearby piles and soil properties on the thermal behaviour of a field-scale energy pile

Aria Moradshahi

PhD student, Monash University, Department of Civil Engineering, 23 College Walk, Clayton, Vic. 3800, Australia. Telephone: +61 3 990 58901; Email: aria.moradshahi@monash.edu

Mohammed Faizal

Research Fellow, Monash University, Department of Civil Engineering, 23 College Walk, Clayton, Vic. 3800, Australia. Telephone: +61 3 9902 9988; Email: mohammed.faizal@monash.edu

*** Abdelmalek Bouazza (Corresponding Author)**

Professor, Monash University, Department of Civil Engineering, 23 College Walk, Clayton, Vic. 3800, Australia. Telephone: +61 3 9905 4956; Email: malek.bouazza@monash.edu

John S. McCartney

Professor and Department Chair, University of California San Diego, Department of Structural Engineering, 9500 Gilman Drive, SME 442J, La Jolla, CA 92093-0085, USA, Telephone: +1 858 534 9630; Email: mccartney@ucsd.edu

Abstract

The thermal response of an energy field scale pile that is part of a pair of energy piles spaced at a centre-to-centre distance of 3.5 m (i.e. 6 D, where D is the pile diameter), was examined experimentally and numerically. Three field tests were conducted to assess the axial and radial thermal responses of the energy pile: (1) heating of the energy pile alone; (2) heating of both energy piles simultaneously, and (3) heating of the other energy pile while the considered energy pile was not heated. Good agreement was obtained between the experimental and numerical evaluations of the energy pile during the tests. A parametric study of the validated numerical model was performed for each of the three tests to understand the effects of varying soil thermal conductivity, thermal expansion coefficient, and elastic modulus on the thermal response of the considered energy pile. The numerical results confirmed the field results that radial thermal stresses in the energy piles were insignificant compared to axial thermal stresses. The impact of elastic modulus of the soil was more significant on the thermal stresses of the energy pile compared to the effects of soil thermal conductivity and thermal expansion coefficient. The thermal stresses of the considered energy pile were not significantly affected when both energy piles were heated simultaneously, even though ground temperature changes between the energy piles were more significant due to thermal interaction. Only minor thermal effects on the non-thermal pile were observed during heating of one of the energy piles for different soil properties.

Keywords: *Energy piles; thermal interaction; field tests;*

Introduction

Energy piles may interact with other energy piles or nearby standard piles through a coupled heat transfer and volume change in the surrounding soil. Although there have been several studies on energy pile groups using field testing and numerical simulations, the role of soil properties on this interaction is not well understood. For example, field studies conducted by Mimouni and Laloui (2015) showed that thermal interactions between thermal and non-thermal piles, for spacing ranging from 3 D to 5 D, could lead to the development of differential thermal loads in the piles. Field studies on a group of 6 energy piles conducted by You et al. (2014) indicated that ground temperatures overlapped between closely spaced (5 D) energy piles. However, the effect of this overlap on the thermal response of the piles was not investigated. Field tests on the axial thermal responses of a group of eight energy piles spaced between 9 m and 12 m (15 D and 20 D) were conducted by Murphy and McCartney (2014) and Murphy et al. (2015). The recorded ground temperatures indicated that the energy piles likely did not interact thermally during the duration of the thermal response tests. Rotta Loria and Laloui (2018) reported the results from field tests on thermal interaction between a triangular-spaced energy pile group with the same spacing as Mimouni and Laloui (2015) that included both operational and non-operational energy piles. They found that higher displacements and lower stresses occurred when all of the energy piles were heated. These observations were confirmed in full-scale tests on a row of energy piles, with 5 D spacing, performed by Wu et al. (2020).

Small-scale physical modelling (Peng et al. 2018; Wu et al. 2018) and numerical and analytical studies (Salciarini et al. 2015; Suryatriyastuti et al. 2016; Saggu and Chakraborty 2016; Di Donna et al. 2016; Rotta Loria and Laloui 2016, 2017a, 2018) highlighted the presence of thermal interactions between energy piles. These studies also reported that the thermal stresses of individual energy piles might be affected up to 50% as a result of thermal interaction with other piles. Most of these previous studies evaluated the axial thermal responses of energy piles, and only Mimouni and Laloui (2015) and Rotta Loria and Laloui (2017b) investigated the radial thermal reactions. A crucial gap in the current literature is that the previous studies did not assess the impact of varying some of the soil properties on the thermal responses of the piles. Some of these properties that could affect the thermal stresses in energy piles are the thermal conductivity, λ_{soil}, thermal expansion coefficient, α_{soil}, and elastic modulus, E_{soil}, of the soil. Studies reported in current literature have investigated the effect of the soil above parameters for single energy piles; however, there is lack of knowledge on how these soil parameters can affect the energy pile thermal responses in case that more than one energy pile is operating.

For instance, the soil thermal conductivity, λ_{soil}, determines the magnitude of conductive heat transfer between the energy pile and the surrounding soils. Guo et al. (2018) and Salciarini et al. (2017) showed that soils with higher λ_{soil} tend to affect the temperature of a larger volume of soil surrounding an energy pile. An increase in λ_{soil} could, therefore, increase the thermal interaction between closely spaced energy piles. Previous numerical studies have indicated that soils with lower λ_{soil} tend to reduce the soil temperature changes due to more moderate heat transfer between the energy pile and the soil, hence leading to an increase in the energy pile temperature (Sani et al. 2019). Numerical studies also reported variations in axial thermal stresses of energy piles (Jeong et al. 2014; Salciarini et al. 2017) when λ_{soil} was varied. These studies indicate that λ_{soil} is a critical parameter that could affect the thermal responses of thermally interacting piles.

The soil thermal expansion coefficient, α_{soil}, determines the magnitude of thermal deformations of the soil when subjected to temperature changes. The soil temperatures between thermally interacting energy piles are anticipated to be higher compared to isolated energy piles; thus, higher soil thermal deformations are also expected (You et al. 2014). The differences in the thermal expansion coefficients of the pile concrete and the soil could affect the magnitudes of thermal stresses developed in the energy pile. This aspect has been highlighted by Rotta Loria and Laloui (2017b) in an experimental and numerical study on an energy pile surrounded by non-thermal piles. They indicated that the axial thermal stresses developed in the energy pile reduced when α_{soil} was higher than that of the pile concrete. Similar observations were reported by Salciarini et al. (2017) for a single energy pile in a group of energy piles and by Bodas Freitas et al. (2013) and Bourne-Webb et al. (2015) on isolated energy piles. Further investigations on the impact of α_{soil} will, therefore, provide more insight into the thermal responses of thermally interacting piles.

The elastic modulus of the soil, E_{soil}, may also affect the thermal responses of energy piles since the restraints to the pile thermal expansion/contraction is affected. A numerical study conducted by Khosravi et al. (2016) showed that an increase in E_{soil} led to the development of higher magnitudes of axial thermal stresses in an energy pile. Olgun et al. (2014) observed that increasing E_{soil} resulted in higher magnitudes of radial contact stresses at the pile-soil interface. These limited studies indicate that variation of E_{soil} could affect the axial and radial thermal responses of energy piles, and is, therefore, a subject of further investigation for thermally interacting piles.

This paper aims to examine the role of soil properties and nearby piles on the thermal behaviour of an energy pile. Field testing and numerical simulations were performed to understand the interaction between a pair of energy piles spaced at a centre-to-centre distance of 3.5 m (6 D). Three scenarios were investigated: (1) heating of the energy pile alone next to a non-operating energy pile; (2) heating of both energy piles simultaneously, and (3) heating of the other energy pile while the considered energy pile was not heated (i.e., a non-operating energy pile). After comparing the results from the experiments and field simulations for the three cases, a parametric evaluation was conducted to explore the effects of varying soil properties (i.e. thermal conductivity, λ_{soil}, thermal expansion coefficient, α_{soil}, and the elastic modulus, E_{soil}) on the thermo-mechanical responses of one of the two energy piles.

In-situ testing

Energy piles description and instrumentation

The soil profile at the test site, summarized in Table 1, consisted of mostly dense sands and was part of the Brighton Group of materials described in detail in Barry-Macaulay et al. (2013) and Faizal et al. (2018; 2019a, 2019b). The site consisted of two cast-in-place bored energy piles with 0.6 m diameter and 10 m length located under a six-storey student residential building at a centre-to-centre distance of 3.5 m (Figure 1). The two energy piles were not linked with a pile-cap. Detailed information on the layout, installation and instrumentation of the energy piles is given in Faizal et al. (2019a). One of the two energy piles (EP1) was instrumented with axial and radial vibrating wire strain gauges and thermocouples. Whereas, the second energy pile (EP2) was only instrumented with three thermocouples on the external wall of the pipes. Four U-shaped heat exchanger loops made with high-density polyethylene (HDPE) pipes were attached to the reinforcing cages up to the depth of both piles. The inner and outer diameters of the HDPE pipes were 20 mm and 25 mm, respectively. The compressive strength and elasticity modulus of the unreinforced concrete measured in the laboratory were 64 MPa and 34 GPa, respectively.

The considered energy pile (EP1) had vibrating wire strain gauges (VWSG) (Model: Geokon-4200) installed at five depths along the pile. There were five axial VWSGs (V1 to V5) and one radial VWSG (R) at each depth. The axial strain gauge V5 and radial strain gauge R were located near the centre of the pile while axial strain gauges V1 to V4 were located at approximately 160 mm away from the pile edge. Average magnitudes of temperatures, strains, and stresses were considered from the axial VWSGs at a given depth. The water temperatures and flow rates at the inlet and outlet of the U-loops were recorded by Type T thermocouples and TM-series digital water flow meters, respectively. The ground temperatures were recorded using Type T thermocouples at two, 12 m deep, boreholes located between the two piles (Figure 1).

Experimental procedure

Three tests were conducted to investigate the aim of this study: (i) heating EP1 only, referred to as $EP1_{active}$, to establish the axial and radial thermal responses of EP1 (ii) heating EP1 and EP2 simultaneously, referred to as $(EP1 + EP2)_{active,}$ to examine the effect of EP2 on the thermal response of EP1 (i.e. to investigate the impact of one operating energy pile on the other operating energy pile), and (iii) heating EP2 only, referred to as $EP2_{active}$ to examine the effect of EP2 as an operating energy pile on the thermal response of EP1 as a nearby non-operating pile). The axial and radial thermal responses of EP1 were monitored in all the experiments due to its substantial instrumentation.

The ambient, inlet water and initial pile and ground temperatures for the three experiments are shown in Figure 2. The atmospheric temperatures used for all the parametric studies were obtained from a weather station located approximately 13 km from the experimental site (Figure 2a). The initial ground temperatures were measured by thermocouples located 0.63 m away from the edge of EP1 (Figure 1). The heating test on EP1 ($EP1_{active}$) lasted for 18 days. Water at 48°C was circulated at a flow rate of 11 l/min in all the four loops. The experimental data for this experiment was reported in Faizal et al. (2019). The heating test on the two piles together, $(EP1 + EP2)_{active}$, lasted for 35 days. The piles were connected in series with a water flow rate of 11 L/min and temperature of 44°C. The heating test on EP2 ($EP2_{active}$) lasted for 40 days with a flow rate of 11 l/min and water temperature of about 46°C. The cases presented herein are for continuous operation of ground source heat pumps that would be applicable to commercial buildings such as hospitals and any other application that require long term heating/cooling.

Numerical modelling

A numerical study was conducted to predict the thermal responses of EP1 for varying soil properties for all the three tests mentioned above. A three-dimensional finite element model was implemented in COMSOL Multiphysics software and was validated with the experimental results. A parametric evaluation of different λ_{soil}, α_{soil}, and E_{soil} was then conducted using the numerical model. The 40×15×30 m^3 3D finite element model, shown in Figure 3, consisted of 344821 tetrahedral, triangular, prismatic, linear and vertex elements from which EP1 is described by 94273 mesh elements.

There was no groundwater encountered within the depth of the pile, and the soil at the site was considered to be dry. The energy piles and the soil were considered to be isotropic, porous media composed of solid particles with voids filled with air, and heat transfer was assumed to be purely conductive. The solid is considered to be incompressible under isothermal conditions. The inertial effects of the solid skeleton are negligible, and the simulations represent quasi-static conditions. The behaviour of all the materials is considered to be linear thermo-elastic, which is a reasonable assumption for relatively stiff soils like those encountered in the energy piles reported in the literature. The governing equations of the coupled thermo-mechanical problem commonly used in energy pile analysis are similar to those adopted by Caulk et al. (2014), Batini et al. (2015), Di Donna et al. (2016), and Rotta Loria and Laloui (2017b). The mechanical equilibrium equation can be written as follows:

$$\mathbf{F}_v = -\nabla.\boldsymbol{\sigma} \quad (1)$$

where F_v is the volume force factor; ∇ indicates divergence; and $\boldsymbol{\sigma}$ is the total stress tensor. The heat conduction equation can be written as follows:

$$(\rho C)_{eff}\frac{\partial T}{\partial t} = -\nabla.\lambda_{eff}\nabla T \quad (2)$$

where T is temperature and $(\rho C)_{eff}$ and λ_{eff} are the effective volumetric heat capacity at constant pressure and effective thermal conductivity, respectively. The thermal properties of the fluid and solid materials were assumed to be temperature-dependent and temperature-independent, respectively. To account for heat transfer in a porous media, the effective volumetric heat capacity $(\rho C)_{eff}$and thermal conductivity λ_{eff} were considered as follows:

$$(\rho C)_{eff} = \theta_p \rho_p C_{p,p} + (1-\theta_p)\rho_s C_{p,s} \quad (3)$$

$$\lambda_{eff} = \theta_p \lambda_p + (1-\theta_p)\lambda_s \quad (4)$$

where $(\rho C)_{eff}$ and λ_{eff} are the effective volumetric heat capacity at constant pressure and effective thermal conductivity, respectively, ρ_p and ρ_s are pore fluid (air in this study) and soil densities, λ_p and λ_s and $C_{p,p}$ and $C_{p,s}$ are representing thermal conductivities and specific heat capacity of these two materials respectively. θ_p is the volume fraction of solid material (the ratio of the area occupied by the pore fluid to the entire cross-section of the soil).

Taking into account the thermal effects, Equation 1 can be rewritten as:

$$\mathbf{F}_v = -\nabla.(C_{ijkl}(\varepsilon_{ij} - \alpha\Delta T)) \quad (5)$$

where C_{ijkl} is the stiffness tensor, which is determined by material properties such as elastic modulus and Poisson's ratio. $\varepsilon_{ij}$is the strain tensor, α is the coefficient of thermal expansion, ΔT is the change in temperature.

The energy conservation equation for water can be written as follows:

$$\rho_f A C_f \frac{\partial T_f}{\partial t} + \rho_f A C_f u_f.\nabla T_f = \nabla.\left(A\lambda_f \nabla T_f\right) + Q_{wall} \quad (6)$$

where ρ_f, C_f, u_f, λ_f and T_f are density, specific heat, velocity vector, thermal conductivity, and temperature of the circulating fluid, respectively. A represents the cross-section of the pipe in which fluid is flowing and Q_{wall} indicates the heat flux per unit length of the pipe and is written as follows:

$$Q_{wall} = h_{eff}(T_{ext} - T_f) \tag{7}$$

where h_{eff} is an effective pipe heat transfer coefficient considering the wetted perimeter of the pipe cross-section; and T_{ext} is the external temperature surrounding the pipe. The effective heat transfer coefficient for circular pipe shapes used in this study can be determined as follows:

$$h_{eff} = \frac{2\pi r_{int}}{\frac{1}{h_{int}} + \frac{r_{int}}{\lambda_p}\ln\left(\frac{r_{ext}}{r_{int}}\right)} \tag{8}$$

where r_{int} and r_{ext} are internal and external pipe radius, respectively; λ_p is pipe thermal conductivity; and h_{int} is convective heat transfer coefficient inside the pipe which can be obtained by:

$$h_{int} = \frac{Nuk_f}{d_h} \tag{9}$$

where d_h is the hydraulic diameter ($d_h = \frac{4A}{2\pi r_{int}}$) and Nu is the Nusselt number for round pipes and can be defined as a function of Reynolds, Re, and Prandtl, Pr, numbers, as follows:

$$Nu = \max\,(3.66; Nu_{turb}) \tag{10.a}$$

$$Nu_{turb} = \frac{\left(\frac{f_D}{8}\right)(Re - 1000)Pr}{1 + 12.7\sqrt{\frac{f_D}{8}}\left(Pr^{\frac{2}{3}} - 1\right)} \tag{10.b}$$

$$f_D = \left[-1.8\log\left(\frac{6.9}{Re}\right)\right]^{-1} \tag{10.c}$$

where f_D is the friction factor; $Re = \rho_f VD/\mu$, $Pr = \mu C_f/\lambda_f$, ρ_f is the fluid density, V is the velocity of the fluid, μ is the dynamic viscosity of the fluid, D is pipe diameter, C_f and λ_f are the specific heat, and the thermal conductivity of the fluid, respectively.

The vertical boundaries at the sides of the model were assigned roller boundary conditions to allow vertical movement of the soil layers. A pinned boundary was applied at the base of the model, which prevents horizontal and vertical movements (Figure 3). The two energy piles and the soil were assumed to be bonded to each other at the pile-soil interface. Each energy pile is connected to a separate slab (with a dimension of 5.0×5.0×0.5 m) with perfect contact (full moment connection). The initial temperatures of the soil, pile, and the pipes were assumed to be the same as the initial ground temperatures recorded at the beginning of each experiment. A design downward concentrated axial load of 1400 kN similar to that of Faizal et al. (2019a,b) was applied at the surface of the slabs above the two pile heads to simulate the building loads. A diffusive surface was applied at the top boundary of the model to account for atmospheric temperature fluctuations which might affect the pile and soil temperatures for depths near the surface.

The soil, energy piles, slab and HDPE pipe properties used in the numerical model were selected based on previous studies conducted on the field site (Barry-Macaulay et al. 2013; Singh et al. 2015; Faizal et al. 2018, 2019a, 2019b) and from common properties reported in the literature (Bowles 1968; Mitchell and Soga 2005; Bourne-Webb et al. 2009; Amatya et al. 2012). These properties are summarized in Table 1.

Field results and numerical validation

The field and numerical results are shown for average temperature changes of EP1, ΔT_{ave} of 10°C and 20°C for both $EP1_{active}$ and $(EP1 + EP2)_{active}$ tests (Figure 4). For $EP1_{active}$, these temperature intervals correspond to 0.67, and 6 days of operation, respectively, and for

(EP1 + EP2)$_{active}$, these intervals correspond to 6.2, and 13.9 days of operation, respectively. For EP2$_{active,}$ the results are shown for the maximum temperature change of 2.2°C of EP1 as a result of EP2 operation, corresponding to 40 days of operation.

The thermal strains, ε_T, were calculated as follows:

$$\varepsilon_T = (\varepsilon_i - \varepsilon_0)B + (T_i - T_0)\alpha_s$$

(**Error! No text of specified style in document.**1)

where ε_i is strain at the time i, ε_o is the initial reference strain, B is the batch calibration factor of the strain gauges with a value of 0.975, T_i is the temperature of the strain gauges at time i, T_o is the reference temperature of the strain gauges, α_s is the coefficient of linear thermal expansion of steel wire in the strain gauges (12.2 με/°C).

The numerical axial and radial contact thermal stresses of EP1 were extracted from the finite element analysis at the pile centre and the pile-soil interface, respectively. The experimental axial thermal stresses in EP1 were estimated by the following equation:

$$\sigma_T = E_P(\varepsilon_{obs} - \alpha_{free}\Delta T) \quad (12)$$

where E_P is the elastic modulus of the concrete (taken as 34 GPa), ε_{obs} is experimentally observed thermal strains, α_{free} is the free thermal expansion coefficient of the concrete, taken as 13 με/°C (Faizal et al., 2019a,b), and ΔT is the change in temperature of the pile. The thermal expansion coefficient of concrete selected in the current study is within the range of 9 με/°C to 14.5 με/°C reported by Stewart and McCartney (2014) and Bourne-Webb et al. (2016).

The experimental radial contact stresses of EP1 were estimated using cavity expansion analysis as follows:

$$\sigma_n = \frac{E_s \Delta r}{(1 + v_s) r} \quad (13)$$

where E_s and v_s are the elastic modulus and Poisson's ratio of the surrounding dense sand, respectively, assumed to be 60 MPa and 0.3, respectively, based on typical values for dense sand (Faizal et al., 2019a,b; Elzeiny et al., 2020), r is the radius of EP1, and Δr is the thermally induced radial displacement of EP1.

The field and numerical results of temperatures, and axial and radial thermal strains/stresses of EP1 plotted against depth, for all experiments, are shown in Figure 4. Positive thermal strains indicate expansion and negative thermal stresses indicate compression. The numerical simulation results matched well with the in-situ results.

The temperatures of EP1 for $EP1_{active}$ and $(EP1 + EP2)_{active}$ tests (shown in Figures 4a and 4b, respectively) were uniform with depth and reached a magnitude of approximately 38°C for both cases. There were negligible differences in the temperatures for EP1 for all tests, indicating that the operation of EP2 has insignificant effects on temperature of EP1 for the given spacing of 3.5 m. The temperature change of EP1 is not significant in the $EP2_{active}$ test compared to the $EP1_{active}$ and $(EP1 + EP2)_{active}$ tests and is also slightly non-uniform with depth, possibly due to some atmospheric effects near the surface. The radial and axial thermal strains (Figures 4c and 4d, respectively) and thermal stresses (Figures 4e and 4f) of EP1 increased when ΔT_{ave} increased from 10°C to 20°C for both $EP1_{active}$ and $(EP1 + EP2)_{active}$ tests. Due to the slight increase in temperature of EP1 in the $EP2_{active}$ test, small variations in axial and radial thermal strains/stresses were also observed in EP1. The lowest magnitude of axial thermal strains (Figure 4d), and thus the highest axial thermal stresses (Figure 4f), were observed at a depth of around 3 m in EP1 for all three experiments. This depth can be considered as the location of the null point, indicating dominant stiffness of the overlying structure relative to the stiffness imposed by the soil beneath the pile toe. The radial thermal strains of EP1 (Figure 4c) were significantly higher than the axial thermal strains of EP1 (Figure 4d) during the

$EP1_{active}$ and $(EP1 + EP2)_{active}$ tests, indicating the energy pile had less restrain to thermal expansion in the radial direction than in the axial direction. As a result, the radial thermal stresses (Figure 4e) were significantly lower than axial thermal stresses (Figure 4f) in EP1 for both $EP1_{active}$ and $(EP1 + EP2)_{active}$ tests.

Figure 5a shows the experimental and numerical change in ground temperatures with depth for $EP1_{active}$ and $(EP1 + EP2)_{active}$ tests at the two boreholes located at 0.63 m and 1.95 m from the edge of EP1 (Figure 1). The ground temperatures at depths of 7.28, 9.5, and 12 m were not recorded from day 7 of the $EP2_{active}$ experiment due to technical issues so the temperature data of this experiment was not shown in Figure 5a. The transient ground temperature changes with increasing radial distance from the sides of EP1 and EP2 for a depth of 5 m is shown in Figure 5b. These ground temperatures are for ΔT_{ave} = 20°C of EP1 for $EP1_{active}$ and $(EP1 + EP2)_{active}$ tests and ΔT_{ave} = 32°C of EP2 in the $EP2_{active}$ test. The ground temperatures at a radial distance of 0 m and 2.9 m from the edge of EP1 are the soil-pile interface temperatures of EP1 and EP2, respectively (Figure 5b). The soil temperature changes between the piles are more significant for the $(EP1 + EP2)_{active}$ test, indicating that heating both piles simultaneously increased the thermal interaction between the piles due to overlapping of ground temperatures. The ground temperature change at the edge of EP2 is lower than at the edge of EP1 in the $(EP1+EP2)_{active}$ test. This is because the heat exchangers of the two piles were connected in series. Since EP1 was heated first, the rate of heating of EP1 was higher than EP2, and the temperature of the fluid entering EP2 was lower than that entering EP1. As a result, EP1 had higher temperature changes than EP2, which resulted in lower temperatures at the edge of EP2. The ground temperatures predicted by numerical simulations matched well with the field results.

Numerical investigation

A parametric evaluation using the validated numerical model was conducted to investigate the effect of soil elastic modulus, E_{soil}, thermal expansion coefficient, α_{soil}, and thermal conductivity, λ_{soil}, on the thermal responses of EP1 for the three field tests described above. Three different values of each soil parameter were considered for all soil layers typical of sandy soil profiles after Bowles (1968) and Mitchel and Soga (2005) (i.e. $0.5E_{soil}$, E_{soil}, $2E_{soil}$; $0.5\lambda_{soil}$, λ_{soil}, $2\lambda_{soil}$; and $0.1\alpha_{soil}$, α_{soil},$10\alpha_{soil}$). The parameters of E_{soil}, λ_{soil}, and α_{soil} have the same magnitudes used for the numerical validation of experimental results (Table 1).

The experimental data for all three field tests had different inlet fluid temperatures, different atmospheric temperatures and different initial pile and ground temperatures (Figure 2). In the parametric study, however, the same test and boundary conditions were applied to all three simulations to assess better the effects of individual soil properties under the same boundary conditions, i.e. same inlet fluid temperatures, fluid velocity (11 L/min), initial pile and ground temperatures, and ambient temperatures. The ambient, inlet fluid and initial pile and ground temperatures used in the parametric study are obtained from $\text{EP1}_{\text{active}}$ test (Figure 2) and are shown in Figure 6. The inlet fluid temperatures represent typical fluid temperatures for energy piles during heating mode of a GSHP.

The parametric simulations were conducted for 14 days for all three field tests. The results in the following sections are presented at Day 14 of the tests. In the parametric evaluation, it was assumed that the two energy piles were working separately (not connected in series) with the same inlet fluid temperatures, as shown in Figure 6b. This was done so that both energy piles had the same inlet fluid temperatures when heated simultaneously. Heating the two piles together in series would reduce the inlet fluid temperatures to EP2 compared to that of EP1 since EP1 will have a faster rate of heating, as was observed in the field test.

Pile and ground temperatures

The effect of varying soil properties on the change in pile temperatures of EP1 and change in ground temperatures between the two piles is shown in Figure 7a and Figure 7b, respectively. The pile temperatures and ground temperatures were not affected by variations in E_{soil} and α_{soil} for all three tests (not shown here). The temperatures of EP1 reduced by approximately 2.5°C when λ_{soil} increased from $0.5\lambda_{soil}$ to $2\lambda_{soil}$ (Figure 7a) for both $\mathrm{EP1}_{\mathrm{active}}$ and $(\mathrm{EP1+EP2})_{\mathrm{active}}$ tests. Higher values of λ_{soil} caused faster heat propagation in the soil, which resulted in lower thermal confinement around EP1, hence lower pile temperatures of EP1 are observed. For a given λ_{soil}, the temperatures of EP1 were same for both $\mathrm{EP1}_{\mathrm{active}}$ and $(\mathrm{EP1+EP2})_{\mathrm{active}}$ tests since the operation of EP2 did not affect the soil temperature at the edge of EP1, even though higher ground temperature changes occurred between the piles when both piles were heated simultaneously, as shown in Figure 7b. No significant changes were observed in temperatures of EP1 for the $\mathrm{EP2}_{\mathrm{active}}$ test. Negative temperature changes of EP1 near the surface during the $\mathrm{EP2}_{\mathrm{active}}$ test is due to the very low atmospheric temperatures at Day 14 (Figure 6a).

The ground temperatures during the $\mathrm{EP1}_{\mathrm{active}}$ test reduced with increasing radial distance from the edge of EP1. The ground temperatures during the $(\mathrm{EP1+EP2})_{\mathrm{active}}$ test also initially reduced with increasing radial distance from the edges of EP1 and EP2, but eventually overlapped and developed higher temperatures near the mid-point between the two energy piles. This overlapping of ground temperatures indicates the presence of thermal interaction between the two energy piles when heated simultaneously in the $(\mathrm{EP1+EP2})_{\mathrm{active}}$ test.

Increasing λ_{soil} reduced the ground temperatures near the energy piles, confirming the findings of Salciarini et al. (2017). This occurred due to higher heat propagation away from the energy piles when λ_{soil} was increased. As a result of faster heat propagation near the piles, the ground temperatures increased farther away from the piles for both $\mathrm{EP1}_{\mathrm{active}}$ and $(\mathrm{EP1+EP2})_{\mathrm{active}}$ tests.

Pile axial thermal strains and stresses

The effect of varying soil properties on the axial thermal strains and stresses of EP1 for all three test conditions are shown in Figure 8. The location of the maximum thermal stresses in EP1 remained approximately at the same depth of 3 m for all studied cases. Varying E_{soil} had more effects on the axial thermal strains and stresses of EP1 compared to the impacts of λ_{soil} and α_{soil} for all three field tests.

The effects of E_{soil} on the axial thermal strains and stresses of EP1 are shown in Figure 8a and Figure 8b, respectively. An increase in E_{soil} significantly increased the axial thermal stresses in EP1 for both $\mathrm{EP1}_{\mathrm{active}}$ and $\mathrm{(EP1{+}EP2)}_{\mathrm{active}}$ tests. Similar observations were noted by Khosravi et al. (2016). The axial thermal stresses in EP1 almost doubled in $\mathrm{EP1}_{\mathrm{active}}$ and $\mathrm{(EP1{+}EP2)}_{\mathrm{active}}$ tests at 3 m depth when E_{soil} increased from $0.5E_{soil}$ to $2E_{soil}$. Higher E_{soil} results in higher rigidity of the soil; hence, a higher restriction is imposed on the axial thermal expansion of the energy pile (Figure 8a). For a given E_{soil}, the thermal stresses developed in EP1 were similar for the $\mathrm{EP1}_{\mathrm{active}}$ and $\mathrm{(EP1{+}EP2)}_{\mathrm{active}}$ tests, with slight differences in the upper section of the pile. This indicates that the operation of one energy pile did not affect the thermal stresses developed in the nearby operating energy pile when both piles were heated simultaneously. Operation of EP2 in the $\mathrm{EP2}_{\mathrm{active}}$ test induced insignificant thermal axial strains and stresses in EP1, indicating that the heating of an energy pile had negligible effects on the nearby non-operating pile. This can be due to the fact that EP1 and EP2 are not connected by a pile-cap. The slightly positive (tensile) axial thermal stresses developed in the upper parts of EP1 in the $\mathrm{EP2}_{\mathrm{active}}$ test (Figure 8b) can be attributed to negative temperature changes in EP1 due to atmospheric effect (see Figure 7a).

Figure 8c and 8d show the effects of λ_{soil} on the axial thermal strains and stresses of EP1, respectively. The thermal stresses developed in EP1 were lower than those developed for different E_{soil}. There was a slight increase in axial thermal stresses of EP1 when λ_{soil} was increased from $0.5\lambda_{soil}$ to $2\lambda_{soil}$ in $EP1_{active}$ and $(EP1+EP2)_{active}$ tests (by approximately 0.3 MPa at 3 m depth), even though the pile temperatures had reduced by 2.5°C (Figure 7a). This could be attributed to the lower expansion of the soil near the pile-soil interface as a result of lower ground temperatures for larger thermal conductivity (Figure 7) which possibly increased restraint of the axial thermal expansion of the pile. The thermal strains and stresses in EP1 were similar for both $EP1_{active}$ and $(EP1+EP2)_{active}$ for any given λ_{soil} with slight differences in the upper pile section, indicating negligible thermal effects of one energy pile on the other when heated simultaneously. The magnitudes of axial thermal stresses and strains in EP1 in the $EP2_{active}$ test were negligible indicating negligible thermal effects on a nearby non-thermal pile due to the operation of an energy pile.

The effects of α_{soil} on the axial thermal strains and stresses of EP1, are shown in Figures 8e and 8f, respectively. The range of thermal stresses was lower than that for E_{soil}. Similar to what was observed for E_{soil} and λ_{soil}, the thermal stresses in EP1 were similar for both $EP1_{active}$ and $(EP1+EP2)_{active}$ test with slight differences in the upper pile section, for a given α_{soil}. Increasing α_{soil} to $10\alpha_{soil}$ (corresponding to $\alpha_{soil}/\alpha_{pile}$ of 0.7 and 7 respectively) resulted in a small reduction in axial thermal stresses in EP1 for both $EP1_{active}$ and $(EP1+EP2)_{active}$ tests, mostly for the upper pile section for $10\alpha_{soil}$ ($\alpha_{soil}/\alpha_{pile}$ of 7). This can be related to the increased soil expansion for higher values of α_{soil} which resulted in a lower restriction on EP1. This behaviour is consistent with the observations reported by Bourne-Webb et al. (2016) and Salciarini (2017). Similar to the effects of E_{soil} and λ_{soil}, there were negligible effects of EP2 operation on EP1 in the $EP2_{active}$ test. The values of $\alpha_{soil}/\alpha_{pile}$ used in this study are consistent with those of other studies which have been reported to vary between 0 and 2 (Bodas Freitas et al., 2013), 0.033 and 3.3 (Rotta Loria and Laloui 2017), and 1 to10 (Salciarini et al. 2017).

Pile radial thermal strains and stresses

The effects of varying soil properties on the radial thermal strains and stresses of EP1 for the three test scenarios are shown in Figure 9. The magnitudes of the radial thermal stresses in EP1 for all investigated soil parameters were significantly lower than the axial thermal stresses shown in Figure 8. The radial thermal strains were more significant and closer to the free thermal expansion of the pile compared to the axial thermal strains reported in Figure 8. These confirm the findings of previous studies that radial thermal stresses are insignificant compared to the magnitudes of axial thermal stresses in energy piles (Ozudogru et al. 2015; Gawecka et al. 2017; Faizal et al. 2018, 2019). The highest magnitudes of radial thermal stresses in EP1 for all cases are at a depth of 3 m due to the higher soil rigidity at this depth. Also, E_{soil} had higher impacts on the radial thermal stresses in EP1 compared to λ_{soil} and α_{soil}.

The effect of E_{soil} on the radial thermal strains and stresses of EP1 are shown in Figures 9a and 9b, respectively. An increase in E_{soil} resulted in an increase in the magnitudes of radial thermal stresses in EP1 in $\mathrm{EP1}_{\mathrm{active}}$ and $(\mathrm{EP1+EP2})_{\mathrm{active}}$ tests due to increased soil rigidity. These observations are consistent with the results reported by Olgun et al. (2014), where the normal stresses increased from 3.5 to 14 kPa when E_{soil} increased from 25 MPa to 100 MPa. For a given E_{soil}, the radial thermal stresses in EP1 were similar for $\mathrm{EP1}_{\mathrm{active}}$ and $(\mathrm{EP1+EP2})_{\mathrm{active}}$ tests, with minor differences of approximately 5 kPa for $2E_{soil}$. This confirms the negligible effects of the operation of one energy pile on the other nearby energy pile for the setting investigated in this study. Insignificant stress changes of up to 2.2 kPa were observed in EP1 during the $\mathrm{EP2}_{\mathrm{active}}$ test.

The effect of λ_{soil} on radial thermal strains and stresses of EP1 are shown in Figures 9c and 9d, respectively. The radial thermal stresses of EP1 slightly reduced when λ_{soil} increased, with a maximum reduction of 4.5 kPa at 3 m depth when λ_{soil} increased from $0.5\lambda_{soil}$ to $2\lambda_{soil}$. No significant differences were observed in radial thermal stresses of EP1 between the $\mathrm{EP1}_{\mathrm{active}}$

and $(EP1+EP2)_{active}$ tests indicating insignificant thermal effects of the operation of one energy pile on the other energy pile. Similar to E_{soil}, negligible stress changes of up to 2.2 kPa were observed in EP1 in the $EP2_{active}$ test.

The effects of α_{soil} on the radial thermal strains and stresses in EP1, are shown in Figures 9e and 9f, respectively. The radial thermal stresses in EP1 increased for both $EP1_{active}$ and $(EP1+EP2)_{active}$ tests with increasing α_{soil}. The radial thermal stresses in EP1 in the $EP1_{actvice}$ test were higher than in the $(EP1+EP2)_{active}$ test for $0.1\alpha_{soil}$ and α_{soil} (corresponding to $\alpha_{soil}/\alpha_{pile}$ of 0.07 and 0.7 respectively). However, for $10\alpha_{soil}$ ($\alpha_{soil}/\alpha_{pile}$ of 7) the opposite behaviour is observed due likely to increased thermal expansion of the soil. A higher volume of soil is subjected to temperature change when both piles are heated together (Rotta Loria and Laloui 2017b). The radial thermal stresses in EP1 during the $EP2_{active}$ test was very low compared to the $EP1_{active}$ and $(EP1+EP2)_{active}$ tests.

Thermal displacements

The effects of varying soil properties on the axial and radial thermal displacements of EP1, for all three test scenarios, is shown in Figure 10. The radial thermal displacements were very low with a range of -0.03 mm to 0.01 mm, for all soil properties. The axial thermal displacements at the pile head of EP1 were much higher than radial thermal displacements and ranged between 0.3 mm to 0.5 mm for all soil properties. The radial and axial thermal displacements of EP1 were, however, up to 0.005% and 0.1% of the pile diameter, respectively, much lower than the generally allowable 10% of the pile diameter failure criteria.

Increasing E_{soil} resulted in a slight decrease in axial thermal displacements of EP1 for both $EP1_{active}$ and $(EP1+EP2)_{active}$ tests due to the higher restriction of the surrounding soil (Figure 11b). The axial thermal displacements of EP1 also reduced with increasing λ_{soil} for both $EP1_{active}$ and $(EP1+EP2)_{active}$ tests, likely due to increased soil strength near the pile due to temperature changes. Increasing α_{soil} did not significantly affect the axial thermal displacement of EP1 for both $EP1_{active}$ and $(EP1+EP2)_{active}$ tests. There were no significant differences in axial and radial thermal displacements of EP1 between the $EP1_{active}$ and $(EP1+EP2)_{active}$ tests for all soil properties, confirming the negligible effects of the operation of one energy pile on the other. The axial and radial thermal displacements of EP1 for the $EP2_{active}$ test were insignificant for all soil properties confirming negligible effects of an operating energy pile on a nearby non-thermal pile

Concluding remarks

This paper examined the thermal responses of one of a pair of field-scale energy piles spaced at a centre-to-centre distance of 3.5 m. A parametric study was conducted with a numerical model validated with field tests to explore the effects of varying soil thermal conductivity, thermal expansion coefficient, and elastic modulus on the thermal response of the considered energy pile. Heating the two piles together increased thermal interaction between the piles due to higher ground temperature changes between the piles due to thermal overlapping. This thermal interaction, however, did not affect the magnitude of thermal stresses developed in the considered energy pile for all soil properties, indicating negligible thermal effects from the operation of one energy pile on the other energy pile during simultaneous heating. Heating only one pile also induced insignificant thermal effects on the other non-thermal pile for all soil properties. This outcome indicates that the operation of energy piles will not induce thermal stresses in nearby non-operating piles in the setting investigated in this paper. The effect of elastic modulus of the soil was more significant on the thermal stresses and displacements developed in the considered energy pile compared to the impact of thermal conductivity and thermal expansion coefficient of the soil. Increasing thermal conductivity of the soil, however, induced higher ground temperature changes around both energy piles. The numerical simulations confirmed the field results that the magnitudes of radial thermal stresses developed energy piles were insignificant compared to the axial thermal stresses for all soil properties. The thermal displacements of the considered energy pile were negligible and significantly lower than 10% of the pile diameter for all studied cases and are not expected to affect the structural integrity of the energy piles. The results of this paper will be useful in assessing the thermal interaction among closely spaced energy piles that are not linked by a pile-cap when designing energy piles at different sites with soil properties similar to those reported in this paper. It should be noted that for energy piles spaced closer to each other (i.e., in secant or tangent walls), thermal interaction between the energy piles might be more significant.

Acknowledgements

This research project was supported under the Australian Research Council's Linkage Projects funding scheme (project number LP120200613). The authors also acknowledge the Australian Government Research Training Program Scholarship provided to the first author. The US National Science Foundation grant CMMI-0928159 supported the fourth author. The support of all the sponsors (Geotechnical Engineering-Acciona, Golder Associates, Geoexchange Australia, Brookfield-Multiplex) is gratefully acknowledged.

References

Abdelaziz, S.L., and Ozudogru, T.Y. 2016. Selection of the design temperature change for energy piles. Applied Thermal Engineering, **107**: 1036-1045. https://doi.org/10.1016/j.applthermaleng.2016.07.067.

Akrouch, G., Sánchez, M., and Briaud, J-L. 2014. Thermo-mechanical behavior of energy piles in high plasticity clays. Acta Geotechnica, **9**(3): 399-412. https://doi.org/10.1007/s11440-014-0312-5.

Amatya, B.L., Soga K., Bourne-Webb P.J. 2012. Thermo-mechanical behaviour of energy piles. Géotechnique, **62**(6):503-519. https://doi.org/10.1680/geot.10.P.116.

Barry-Macaulay, D., Bouazza, A., Singh, R., Wang, B., and Ranjith, P. 2013. Thermal conductivity of soils and rocks from the Melbourne (Australia) region. Engineering Geology, **164**: 131-138. https://doi.org/10.1016/j.enggeo.2013.06.014.

Batini, N., Rotta Loria, A.F., Conti, P., Testi, D., Grassi, W. and Laloui, L. 2015. Energy and geotechnical behaviour of energy piles for different design solutions. Computers and Geotechnics, **86** (1): 199–213. https://doi.org/10.1016/j.applthermaleng.2015.04.050.

Bodas Freitas, T., Cruz Silva, F., and Bourne-Webb, P.J. 2013. The response of energy foundations under thermo-mechanical loading. In Proceedings of 18th international conference on soil mechanics and geotechnical engineering, **4**: 3347-3350. Paris, France: Comité Français de Mécanique des Sols et de Géotechnique.

Bourne-Webb, P.J., B. Amatya, K. Soga, T. Amis, C. Davidson, and P. Payne. 2009. Energy pile test at Lambeth College, London: Geotechnical and thermodynamic aspects of pile response to heat cycles. Géotechnique, **59**(3): 237–248. https://doi.org/10.1680/geot.2009.59.3.237.

Bourne-Webb, P.J., Bodas Freitas, T.M., and Freitas Assunção, R. M. 2015. Soil–pile thermal interactions in energy foundations. Géotechnique, **66**(2): 167-171. https://doi.org/10.1680/jgeot.15.T.017.

Bowles, Joseph E. 1968. Foundation analysis and design. New York: McGraw-Hill

Caulk, R., Ghazanfari, E., and McCartney, J.S. 2016. Parameterization of a calibrated geothermal energy pile model. Geomechanics for Energy and the Environment, **5**: 1-15. https://doi.org/10.1016/j.gete.2015.11.001.

Di Donna, A., Rotta Loria, A.F., and Laloui, L. 2016. Numerical study of the response of a group of energy piles under different combinations of thermo-mechanical loads.

Computers and Geotechnics, **72**: 126-142. https://doi.org/10.1016/j.compgeo.2015.11.010.

Elzeiny, R., Suleiman, M. T., Xiao, S., Abu Qamar, M. A., and Al-Khawaja, M. (2020). Laboratory-Scale Pull-Out Tests on a Geothermal Energy Pile in Dry Sand Subjected to Heating Cycles. Canadian Geotechnical Journal, (ja). https://doi.org/10.1139/cgj-2019-0143.

Faizal, M., Bouazza, A., and Singh, R. M. 2016. An experimental investigation of the influence of intermittent and continuous operating modes on the thermal behaviour of a full scale geothermal energy pile. Geomechanics for Energy and the Environment, **8**: 8-29. https://doi.org/10.1016/j.gete.2016.08.001.

Faizal, M., Bouazza, A., Haberfield, C., and McCartney J.S. 2018. Axial and radial thermal responses of a field-scale energy pile under monotonic and cyclic temperature changes. Journal of Geotechnical and Geoenvironmental Engineering, **144**(10): 04018072. https://doi.org/10.1139/cgj-2018-0246.

Faizal, M., Bouazza, A., McCartney, J.S., and Haberfield, C. 2019a. Axial and radial thermal responses of an energy pile under a 6-storey residential building. Canadian Geotechnical Journal, **56**(7): 1019–1033. https://doi.org/10.1061/(ASCE)GT.1943-5606.0001952.

Faizal, M., Bouazza, A., McCartney, J.S. and Haberfield, C. 2019b. Effects of cyclic temperature variations on the thermal response of an energy pile under a residential building. Journal of Geotechnical and Geoenvironmental Engineering **145** (10): 04019066. https://doi.org/10.1061/(ASCE)GT.1943-5606.0002147

Gawecka, K.A., Taborda, D.M.G., Potts, D.M., Cui, W., Zdravković, L., and Kasri, M.S.H. 2017. Numerical modelling of thermo-active piles in London Clay. Proceedings of the Institution of Civil Engineers - Geotechnical Engineering, **170**(3): 201-219.

Gnielinski, V. 1975. New equations for heat and mass transfer in the turbulent flow in pipes and channels. NASA STI/recon technical report A, **75**: 8-16.

Guo, Y., Zhang, G., and Liu, S. 2018. Investigation on the thermal response of full-scale PHC energy pile and ground temperature in multi-layer strata. Applied Thermal Engineering, **143**: 836–848. https://doi.org/10.1016/j.applthermaleng.2018.08.005.

Haaland, S.E. 1983. Simple and explicit formulas for the friction factor in turbulent pipe flow. Journal of Fluids Engineering, **105**(1): 89-90.

Hamada, Y., Saitoh, H., Nakamura, M., Kubota, H., and Ochifuji, K. 2007. Field performance of an energy pile system for space heating. Energy and Buildings, **39**(5): 517-524. https://doi.org/10.1016/j.enbuild.2006.09.006.

Jeong, S., Lim, H., Lee, J.K., and Kim, J. 2014. Thermally induced mechanical response of energy piles in axially loaded pile groups. Applied Thermal Engineering, **71**(1): 608-615. https://doi.org/10.1016/j.applthermaleng.2014.07.007.

Khosravi, A., Moradshahi, A., McCartney, J.S., and Kabiri, M. 2016. Numerical analysis of energy piles under different boundary conditions and thermal loading cycles. E3S Web Conference, **9**: 05005. EDP Sciences.

Laloui, L., Nuth, M., and Vulliet, L. 2006. Experimental and numerical investigations of the behaviour of a heat exchanger pile. International Journal for Numerical and Analytical Methods in Geomechanics, **30**(8): 763-781. https://doi.org/10.1002/nag.499.

McCartney, J.S. and K.D. Murphy 2012. Strain distributions in full-scale energy foundations. DFI Journal - The Journal of the Deep Foundations Institute, **6**(2): 26-38. https://doi.org/10.1179/dfi.2012.008.

McCartney, J.S., and Murphy, K.D. 2017. Investigation of potential dragdown/uplift effects on energy piles. Geomechanics for Energy and the Environment, **10**: 21-28. https://doi.org/10.1016/j.gete.2017.03.001.

Mimouni, T., and Laloui, L. 2015. Behaviour of a group of energy piles. Canadian Geotechnical Journal, **52**(12): 1913-1929. https://doi.org/10.1139/cgj-2014-0403.

Mitchell, J.K. and Soga, K. 2005. Fundamentals of soil behavior, 3rd edition. Wiley, New Jersey.

Murphy, K.D., and McCartney, J.S. 2014. Seasonal response of energy foundations during building operation. Geotechnical and Geological Engineering, **33**(2): 343-356. https://doi.org/10.1007/s10706-014-9802-3.

Murphy, K.D., McCartney, J.S., and Henry, K. S. 2015. Evaluation of thermo-mechanical and thermal behavior of full-scale energy foundations. Acta Geotechnica, **10**(2): 179-195. https://doi.org/10.1007/s11440-013-0298-4.

Olgun, C., Ozudogru, T., and Arson. 2014. Thermo-mechanical radial expansion of heat exchanger piles and possible effects on contact pressures at pile–soil interface. Géotechnique Letters, **4**(3): 170-178. https://doi.org/10.1680/geolett.14.00018.

Ozudogru, T.Y., Olgun, C.G., and Arson, C.F. 2015. Analysis of friction induced thermo-mechanical stresses on a heat exchanger pile in isothermal soil. Geotechnical and Geological Engineering, **33**(2): 357-371. https://doi.org/10.1007/s10706-014-9821-0.

Peng, H.F., Kong, G.Q., Liu, H.L., Abuel-Naga, H., and Hao, Y. H. 2018. Thermo-mechanical behaviour of floating energy pile groups in sand. Journal of Zhejiang University-SCIENCE A, **19**(8): 638-649. https://doi.org/10.1631/jzus.A1700460.

Ravera, E., Sutman, M. and Laloui, L., 2019. Analysis of the interaction factor method for energy pile groups with slab. Computers and Geotechnics, p.103294. https://doi.org/10.1016/j.compgeo.2019.103294.

Rotta Loria, A.F. and Laloui, L. 2016. The interaction factor method for energy pile groups. Computers and Geotechnics, **80**: 121-137. https://doi.org/10.1016/j.compgeo.2016.07.002.

Rotta Loria, A.F. and Laloui, L. 2017a. The equivalent pier method for energy pile groups. Géotechnique, **67**(8): 691–702. https://doi.org/10.1680/jgeot.16.P.139.

Rotta Loria, A.F. and Laloui, L. 2017b. Thermally induced group effects among energy piles. Géotechnique, **67**(5): 374-393. https://doi.org/10.1680/jgeot.16.P.039.

Rotta Loria, A. F. and Laloui, L. 2018. Group action effects caused by various operating energy piles. Géotechnique, **68**(9): 834-841. https://doi.org/10.1680/jgeot.17.P.213.

Saggu, R., and Chakraborty, T. 2016. Thermo-mechanical response of geothermal energy pile groups in sand. International Journal of Geomechanics, **16**(4): 04015100. https://doi.org/10.1061/(ASCE)GM.1943-5622.0000567.

Salciarini, D., Ronchi, F., Cattoni, E., and Tamagnini, C. 2015. Thermo-mechanical effects induced by energy piles operation in a small piled raft. International Journal of Geomechanics, **15**(2): 04014042. https://doi.org/10.1061/(ASCE)GM.1943-5622.0000375.

Sani, A.K., Singh, R.M., Tsuha, C.de H.C., and Cavarretta, I. (2019). Pipe–pipe thermal interaction in a geothermal energy pile. Geothermics, **81**: 209–223. https://doi.org/10.1016/j.geothermics.2019.05.004.

Singh, R., Bouazza, A., and Wang, B. 2015. Near-field ground thermal response to heating of a geothermal energy pile: Observations from a field test. Soils and Foundations, **55**(6): 1412-1426. https://doi.org/10.1016/j.sandf.2015.10.007.

Stewart, M. A., and McCartney, J. S. 2014. Centrifuge modeling of soil-structure interaction in energy foundations. Journal of Geotechnical and Geoenvironmental Engineering, **140**(4): 04013044-1-11. https://doi.org/10.1061/(ASCE)GT.1943-5606.0001061.

Suryatriyastuti, M.E., Mroueh, H., and Burlon, S. 2012. Understanding the temperature-induced mechanical behaviour of energy pile foundations. Renewable and Sustainable Energy Reviews, **16**(5): 3344-3354. https://doi.org/10.1016/j.rser.2012.02.062.

Suryatriyastuti, M.E., Burlon, S., and Mroueh, H. 2016. On the understanding of cyclic interaction mechanisms in an energy pile group. International Journal for Numerical and Analytical Methods in Geomechanics, **40**(1): 3-24. https://doi.org/10.1002/nag.2382.

Sutman, M., Brettmann, T. and Olgun, C.G., 2019. Full-scale in-situ tests on energy piles: Head and base-restraining effects on the structural behaviour of three energy piles. Geomechanics for Energy and the Environment, **18**: 56-68. https://doi.org/10.1016/j.gete.2018.08.002.

You, S., Cheng, X., Guo, H., and Yao, Z. 2014. In-situ experimental study of heat exchange capacity of CFG pile geothermal exchangers. Energy and Buildings, **79**: 23-31. https://doi.org/10.1016/j.enbuild.2014.04.021.

Wang, B., Bouazza, A., Singh, R.M., Haberfield, C., Barry-Macaulay, D., and Baycan, S., 2015. Posttemperature effects on shaft capacity of a full-scale geothermal energy pile. Journal of Geotechnical and Geoenvironmental Engineering, **141**(4): 04014125. https://doi.org/10.1061/(ASCE)GT.1943-5606.0001266.

Wu, D., Liu, H.L., Kong, G.Q., Ng, C.W.W., and Cheng, X.H. 2018. Displacement response of an energy pile in saturated clay. Proceedings of the Institution of Civil Engineers-Geotechnical Engineering, **171**(4): 285-294. https://doi.org/10.1680/jgeen.17.00152.

Wu, D., Liu, H., Kong, G., and Ng, C.W.W. (2020). Interactions of an energy pile with several traditional piles in a row. Journal of Geotechnical and Geoenvironmental Engineering, **146**(4). https://doi.org/10.1061/(ASCE)GT.1943-5606.0002224.

LIST OF FIGURE CAPTIONS

Figure 1. Field scale energy piles instrumentation and WVSGs locations (after Faizal et al. 2019).

Figure 2. Inlet water temperatures during the three experiments.

Figure 3. Finite element mesh of the numerical model (a) 3D view; (b) plan view; (c) side view of energy pile and heat exchanger loops; (d) plan view of energy pile and heat exchanger loops.

Figure 4. Experimental and numerical profiles of EP1 (a) temperatures from radial VWSGs; (b) temperatures from axial VWSGs; (c) radial thermal strains; (d) axial thermal strains; (e) radial thermal stresses; (f) axial thermal stresses.

Figure 5. Experimental and numerical soil temperature distributions between the two energy piles: (a) versus depth; (b) versus radial distance at a depth of 5 m.

Figure 6. Ambient and inlet fluid temperatures used in the parametric analyses: (a) ambient atmospheric temperature; (b) inlet fluid temperature.

Figure 7. Effect of varying soil thermal conductivity on (a) EP1 temperature; (b) ground temperature.

Figure 8. Axial thermal responses of EP1 from the parametric evaluation: (a) strains when varying E_{soil}; (b) stresses when varying E_{soil}; (c) strains when varying λ_{soil}; (d) stresses when varying λ_{soil}; (e) strains when varying α_{soil}; (f) stresses when varying α_{soil}.

Figure 9. Radial thermal responses of EP1 from the parametric evaluation: (a) strains when varying E_{soil}; (b) stresses when varying E_{soil}; (c) strains when varying λ_{soil}; (d) stresses when varying λ_{soil}; (e) strains when varying α_{soil}, (f) stresses when varying α_{soil}.

Figure 10. Radial (δ_{TR}) and axial (δ_{TA}) thermal displacements of EP1 from the parametric evaluation: (a) δ_{TR} when varying E_{soil}; (b) δ_{TA} when varying E_{soil}; (c) δ_{TR} when varying λ_{soil}; (d) δ_{TA} when varying λ_{soil}; (e) δ_{TR} when varying α_{soil}; (f) δ_{TA} when varying α_{soil}.

LIST OF TABLES

Table 1. Material properties for numerical simulations calibrated against field test measurements

Table 1. Material properties for numerical simulations calibrated against field test measurements

Material	Depth z [m]	Elastic modulus E [MPa]	Poisson's ratio ν [—]	Porosity n [—]	Total density ρ [kg/m^3]	Specific heat C_p [J/kgK]	Thermal Conductivity λ [W/(mK)]	Coef. Therm. Exp. α [με/°C]
Fill	0.0-0.5	15	0.3	0.35	1750	800	1.1	10
Sand	0.5-3.5	500	0.25	0.33	1800	840	1.7	10
Sandy clay	3.5-6.0	75	0.30	0.33	1950	810	2.0	10
Sand	6.0-12.5	120	0.25	0.30	2200	850	2.3	10
Pile	—	35000	0.22	—	2500	810	1.5	13
Slab	—	35000	0.20	—	2500	850	1.5	13
HDPE pipes	—	—	—	—	—	—	0.4	—

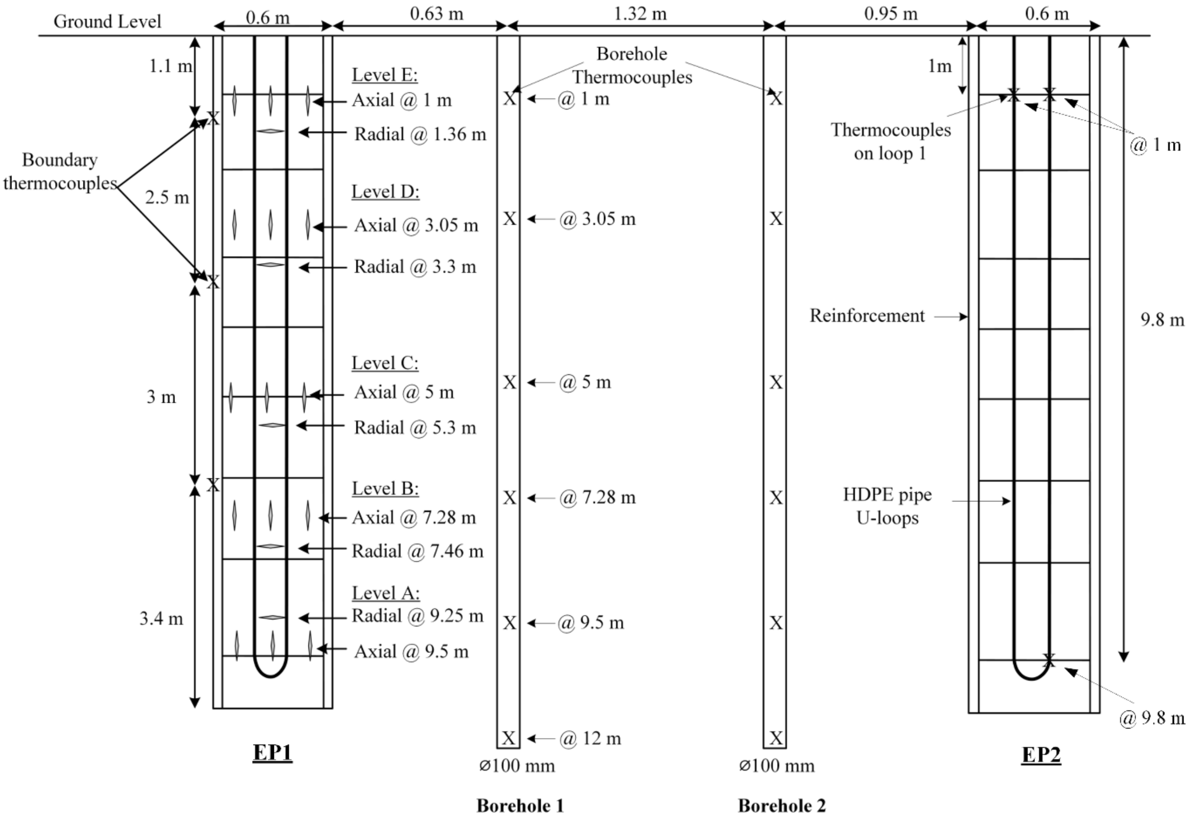

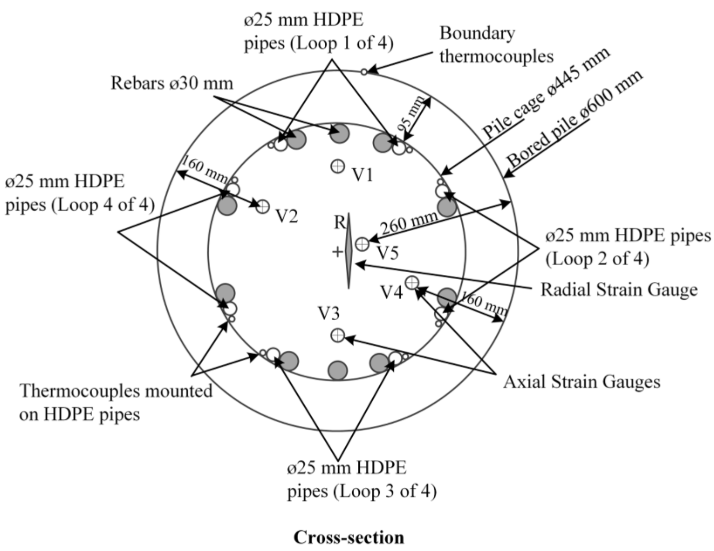

Figure 1. Field scale energy piles instrumentation and WVSGs locations (after Faizal et al. 2019).

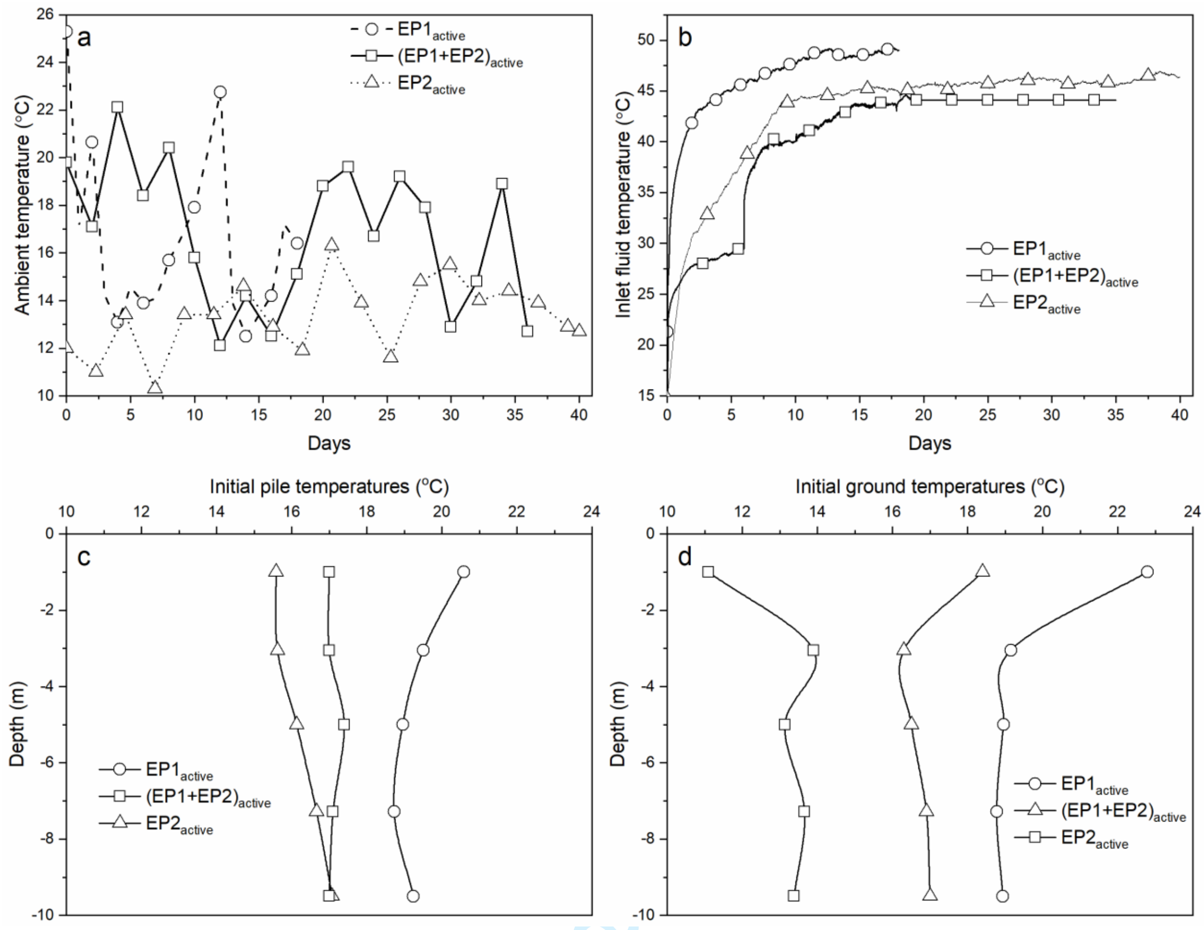

Figure 2. Ambient, inlet fluid temperature, and initial pile and ground during three experiments: (a) ambient atmospheric temperature; (b) inlet fluid temperature; (c) initial pile temperatures; and (d) initial ground temperatures.

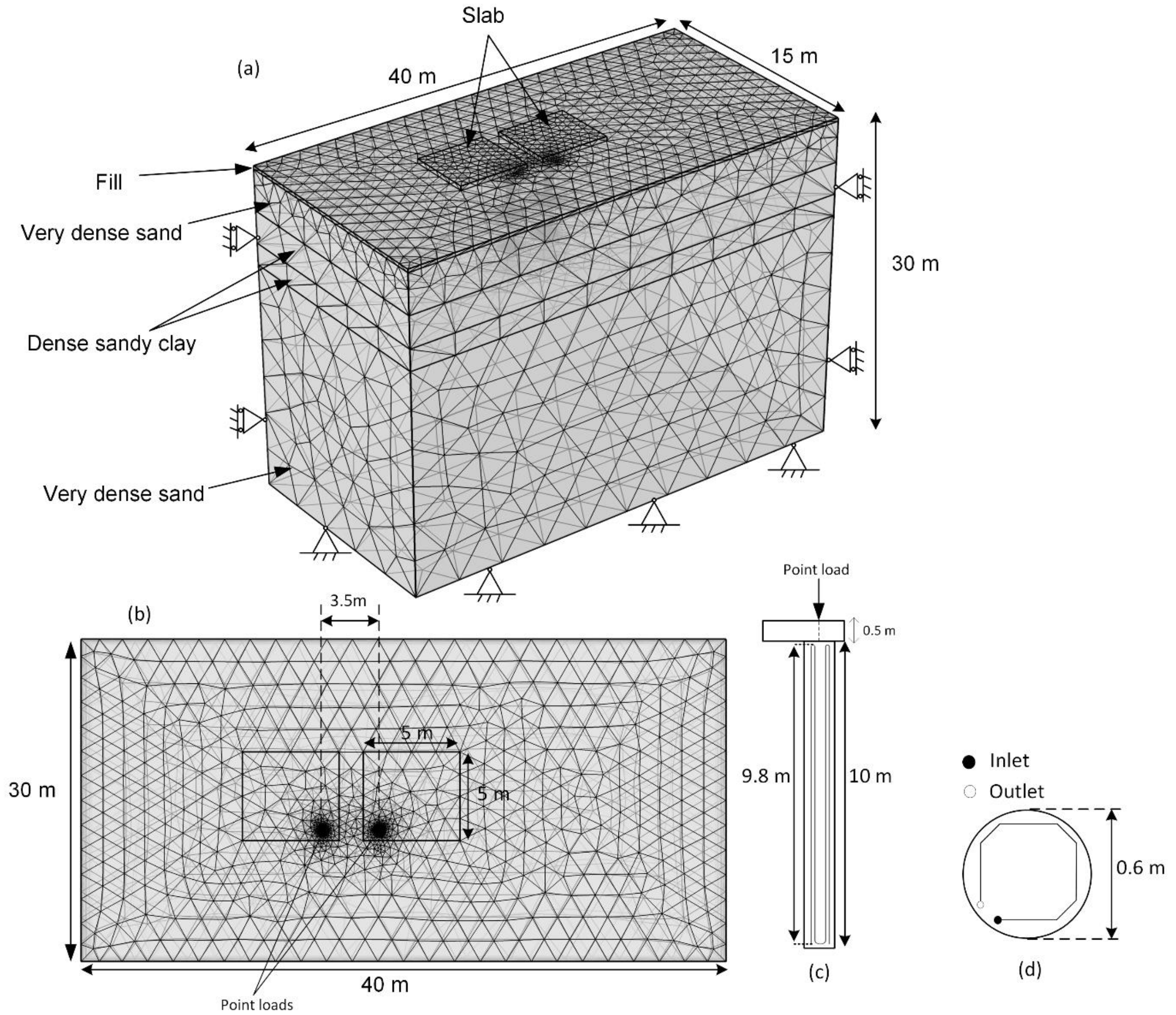

Figure 3. Finite element mesh of the numerical model (a) 3D view; (b) plan view; (c) side view of energy pile and heat exchanger loops; (d) plan view of energy pile and heat exchanger loops.

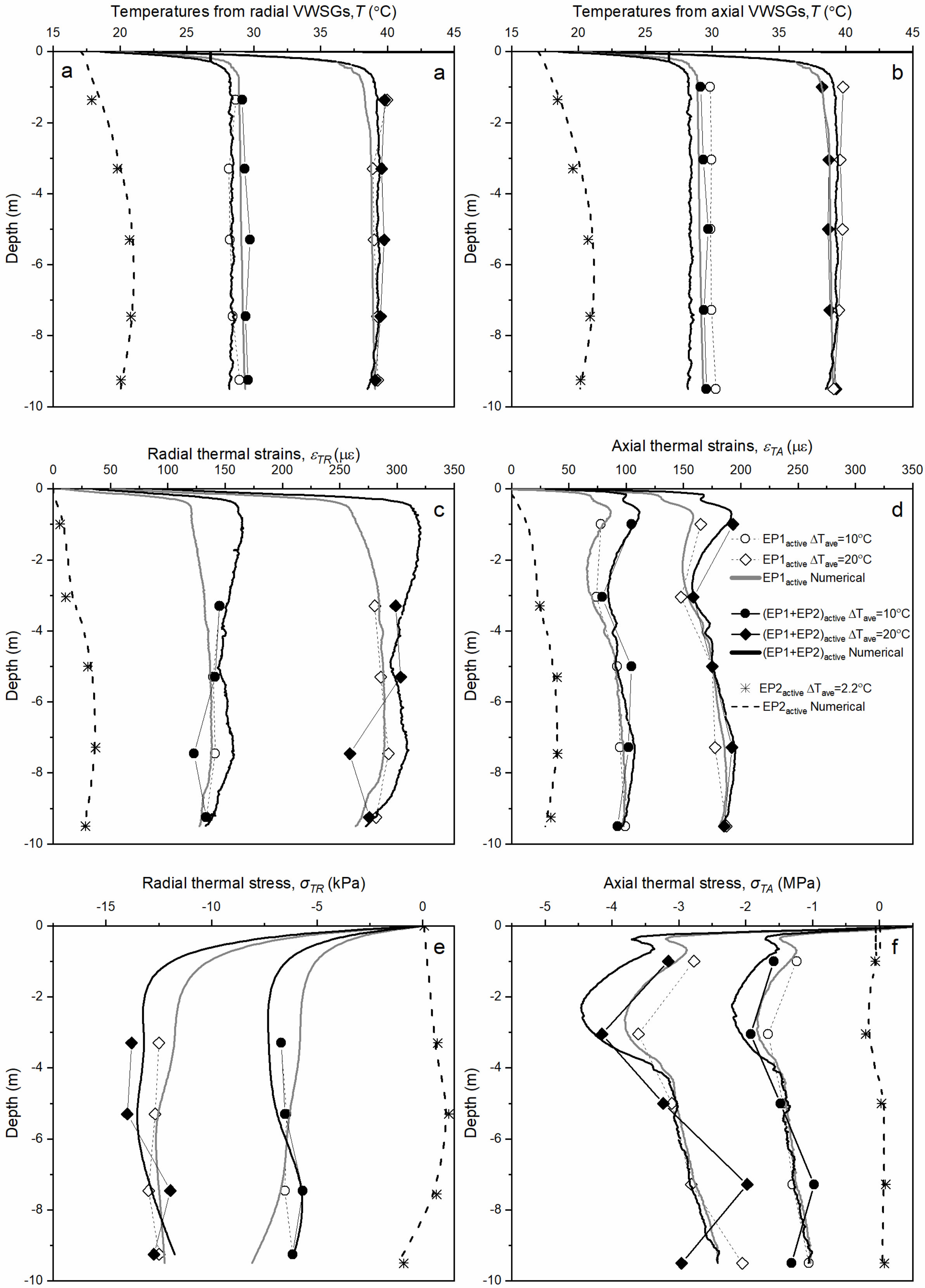

Figure 4. Experimental and numerical profiles of EP1 (a) temperatures from radial VWSGs; (b) temperatures from axial VWSGs; (c) radial thermal strains; (d) axial thermal strains; (e) radial thermal stresses; (f) axial thermal stresses.

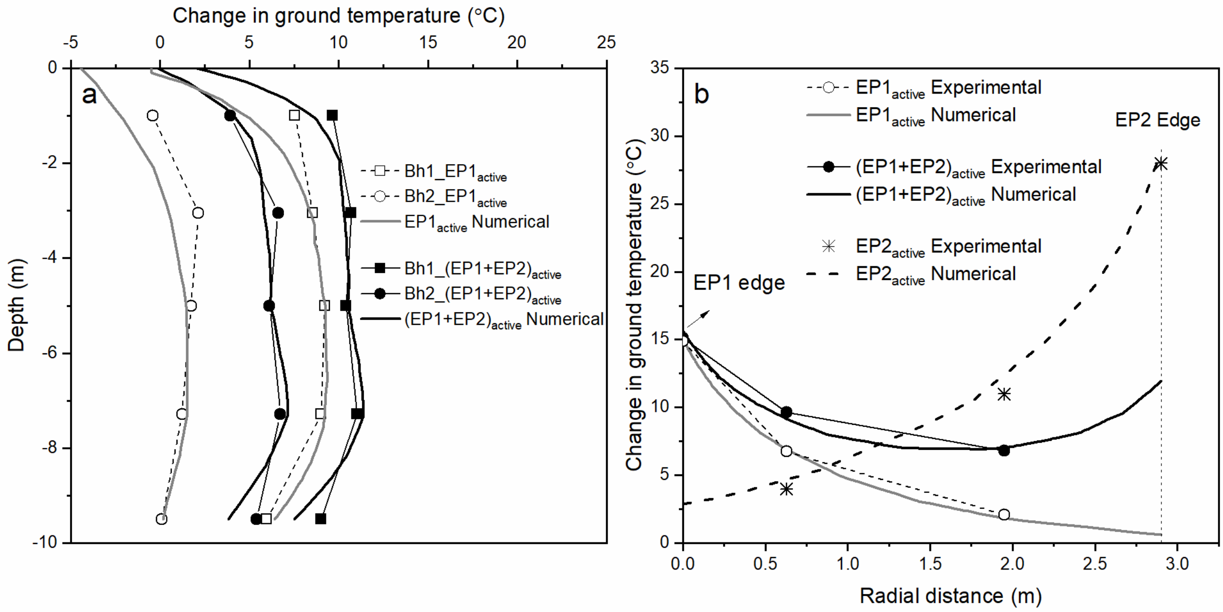

Figure 5. Experimental and numerical soil temperature distributions between the two energy piles: (a) versus depth; (b) versus radial distance at a depth of 5 m.

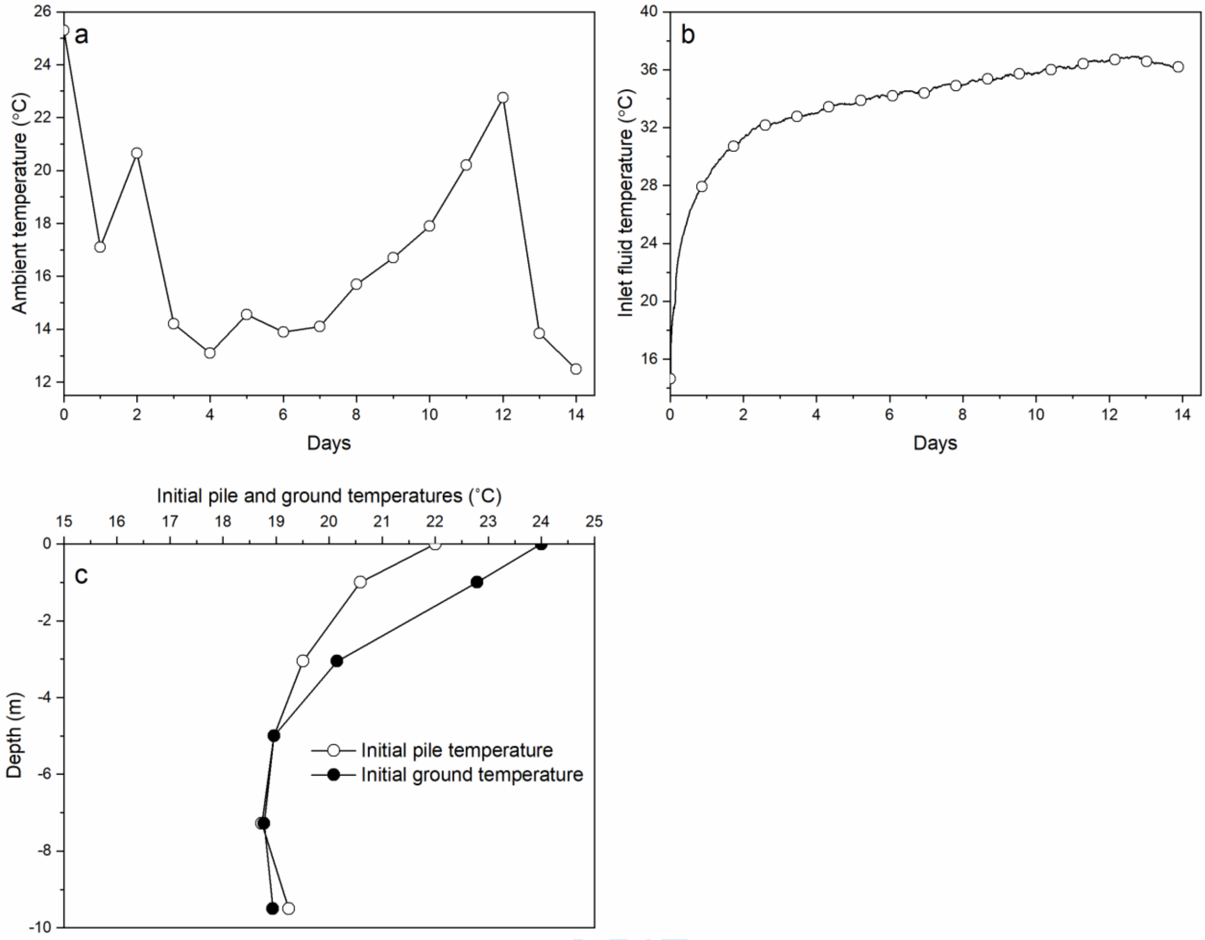

Figure 6. Ambient, inlet fluid temperature, and initial pile and ground temperature used in the parametric analyses: (a) ambient atmospheric temperature; (b) inlet fluid temperature; and (c) initial pile and ground temperatures.

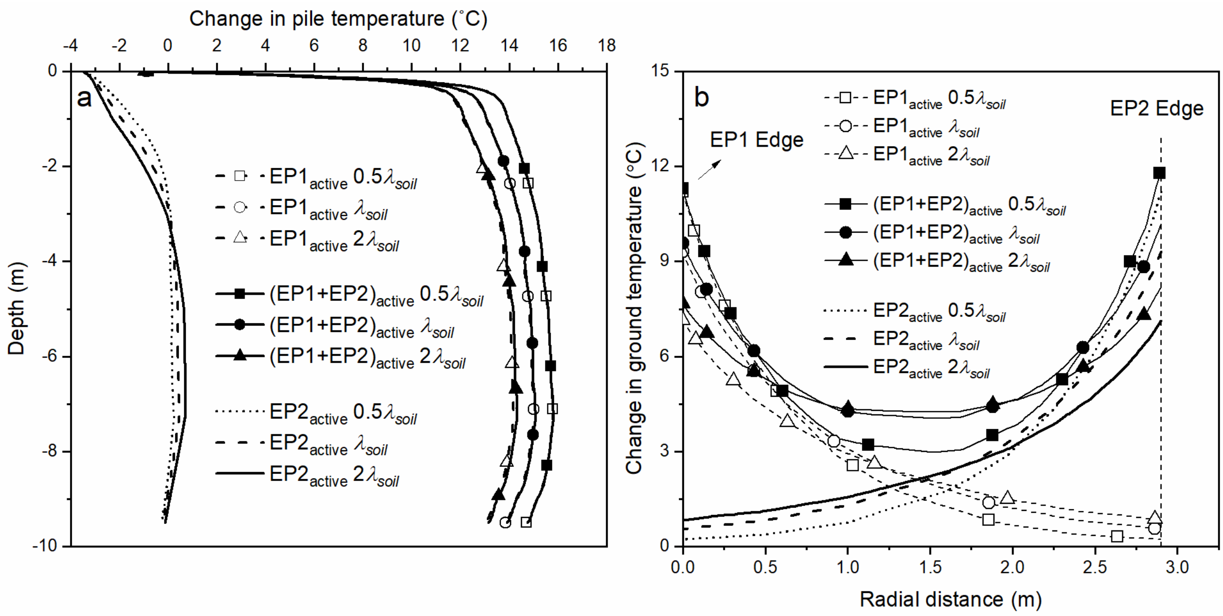

Figure 7. Effect of varying soil thermal conductivity on (a) EP1 temperature; (b) ground temperature.

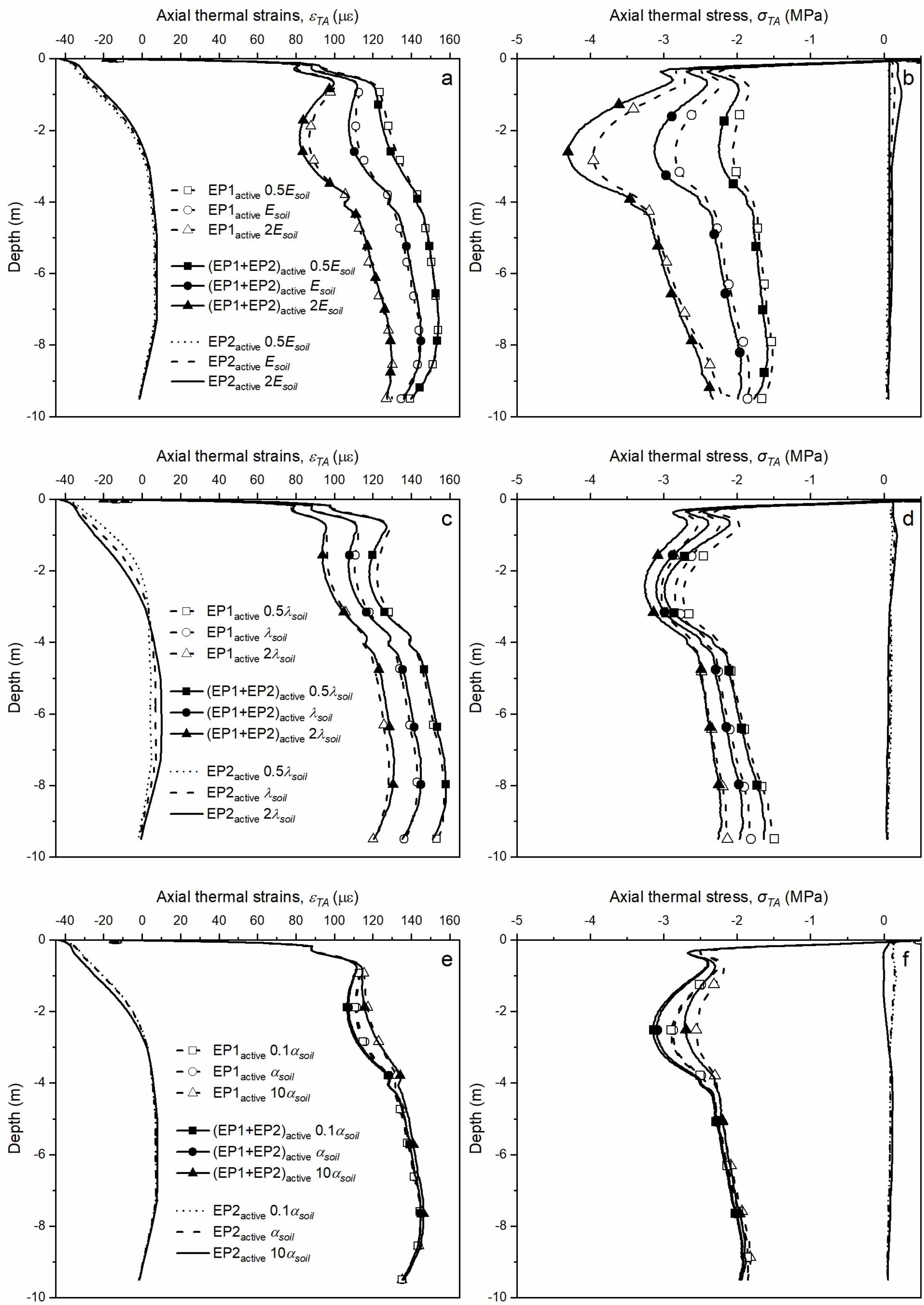

Figure 8. Axial thermal responses of EP1 from the parametric evaluation: (a) strains when varying E_{soil}; (b) stresses when varying E_{soil}; (c) strains when varying λ_{soil}; (d) stresses when varying λ_{soil}; (e) strains when varying α_{soil}; (f) stresses when varying α_{soil}.

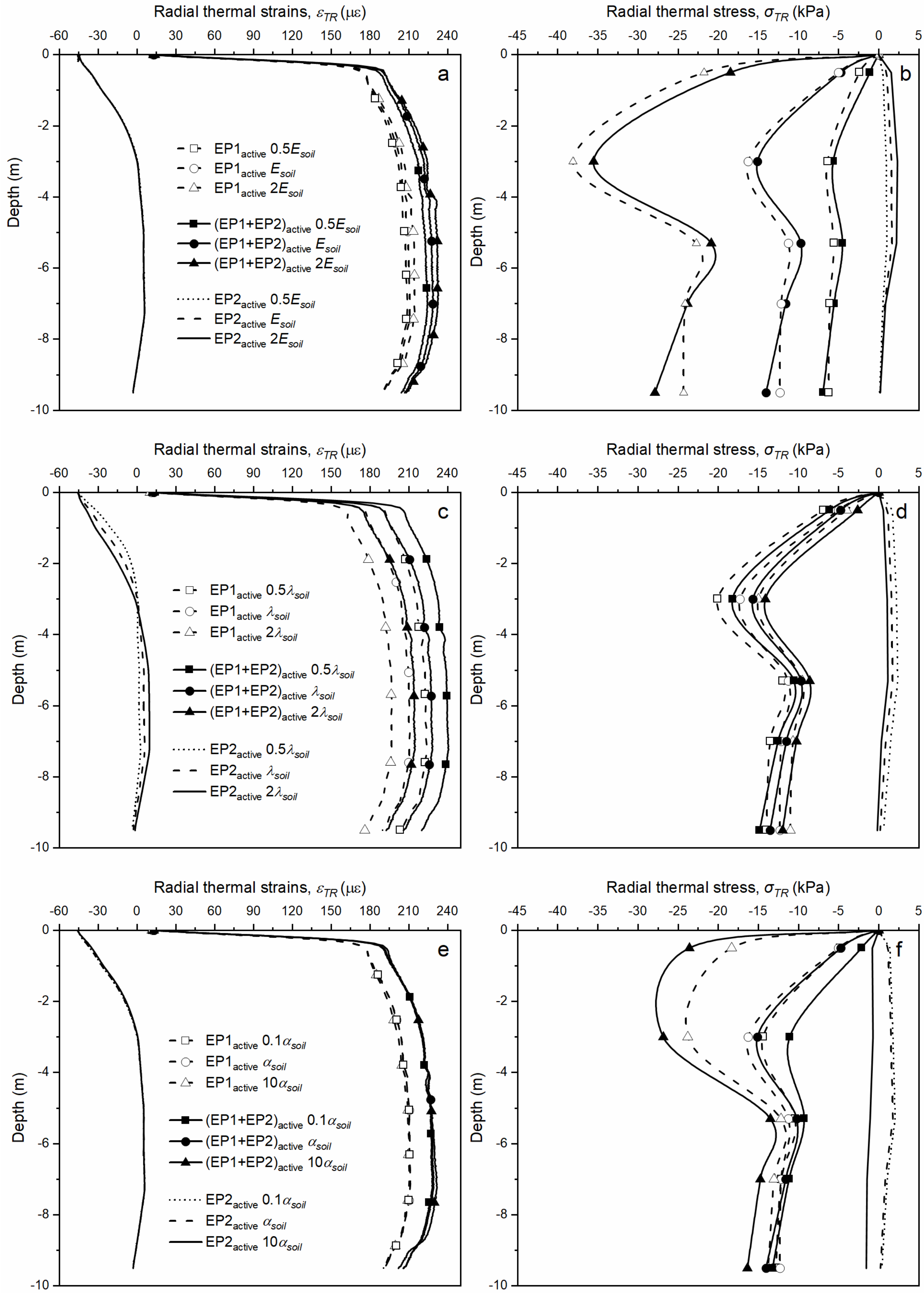

Figure 9. Radial thermal responses of EP1 from the parametric evaluation: (a) strains when varying E_{soil}; (b) stresses when varying E_{soil}; (c) strains when varying λ_{soil}; (d) stresses when varying λ_{soil}; (e) strains when varying α_{soil}, (f) stresses when varying α_{soil}.

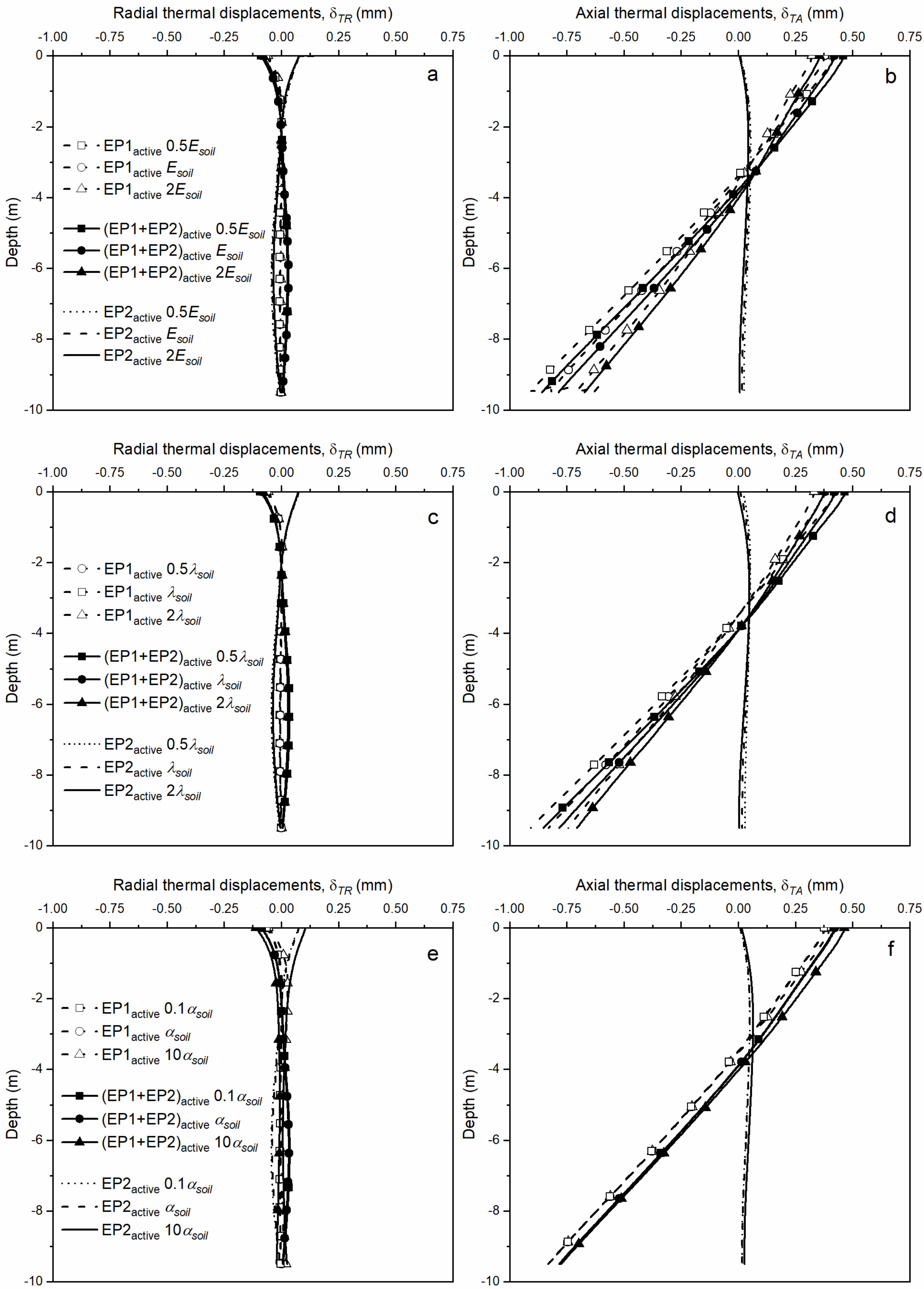

Figure 10. Radial (δ_{TR}) and axial (δ_{TA}) thermal displacements of EP1 from the parametric evaluation: (a) δ_{TR} when varying E_{soil}; (b) δ_{TA} when varying E_{soil}; (c) δ_{TR} when varying λ_{soil}; (d) δ_{TA} when varying λ_{soil}; (e) δ_{TR} when varying α_{soil}; (f) δ_{TA} when varying α_{soil}.